

Closed loop fiber optical gyroscopes for commercial and space applications

**Yu. Korkishko, V.Fedorov, V.Prilutskii, V.Ponomarev, I.Morev,
S.Kostritskii, A.Zuev, V.Varnakov**

¹ RPC OPTOLINK
Sosnovaya alley, premises 2, bld.6A, Zelenograd, Moscow 124489
Russian Federation
Tel.+7495-6631760, fax.+7495-6631761, e-mail:opto@optolink.ru

Abstract

The design and industrial production of closed loop fiber optical gyroscopes with linear digital output for commercial, military and space applications is considered. These gyros characterized by high accuracy can be applied in high-grade (space, aviation, marine, land) inertial navigation systems.

1. Introduction

Over the last twenty years, the interferometric fiber-optic gyroscope (IFOG) has evolved from pioneering physics experiment to a practical device that is now in production. Today, it is now accepted among inertial guidance and navigation specialists that IFOG is strong contender for many civilian, military and space applications. IFOGs are well known as sensors for rotation, which are based on Sagnac effect [1], and have been under development for a number of years to meet a wide range of performance requirements.

2. Results

2.1. Configuration of commercial IFOG.

Optolink Ltd. designed and started the industrial fabrication of the family of closed loop interferometric fiber optical gyroscopes (IFOG) worked as a sensor of rotation rate more than 10 years ago [4]. Both 1-axis and 3-axis IFOGs have been developed and produced now [4-13]. Our IFOGs have so-called minimum configuration (Figs.1,2) that provides reciprocal optical paths for two beams counter-propagating in a fiber loop. The IFOG consists of the one Light Source (Superluminescent diode (SLD)), Photodetectors (PD), circulators (C) and PM Fiber Couplers (PMC) to divide the light into two or three parts, one or three sets of ring interferometers to sense one or three orthogonal angular rate, and printed circuit boards installed signal processing circuits. The ring interferometer consists of a multifunction integrated optic chip (MIOC) and polarization maintaining (PM) fiber coil. Both, MIOC and PM fiber are industrially fabricated by RPC Optolink. The MIOC is a three-port optical gyrochip fabricated at lithium niobate wafer by high temperature proton exchange technique [2]. PM fiber is used in order to reduce both the drift caused by the polarization cross coupling and the drift caused by earth's and outside magnetic field via the Faraday effect. The SLD generates the light that would pass through circulator and splits evenly into two ways at the Y-junction of the MIOC. The two waves travel inside the fiber sensing coil in clockwise and counter-wise directions respectively, then interfere back at the Y-junction and arrive at the photodetector module through circulator. When the

system is a subject of rotation, the two waves experience a phase difference because of the different optical path lengths:

$$\varphi_s = \frac{2\pi LD}{\lambda c} \Omega = \frac{2\pi^2 D^2 N}{\lambda \cdot c} \Omega \quad (1)$$

where L is the coil length, D- coil diameter, N- number of coil turns, λ - is the wavelength and c is the light speed.

Depending on sensitivity, bias drift and dynamic range, different types of Optolink's gyros contain from 200 m to 2000 m long fiber optical coil, made from self-produced single mode at 1550 nm wavelength PM fiber (PANDA type). The fiber coils are fabricated by symmetrical winding with stable stretch. The coil is placed at temperature isolated plate with diameter from 60 to 230 mm depending on type of IFOG. PIN photodiodes are used as a PD, and pigtailed temperature stabilized SLD with output power from 10 to 20 mW is used as a light source. Stabilization of temperature of SLD by Pelletier module enables one to achieve temperature stability of IFOG's scale factor. Our 3-Axis IFOG adopts just one light source for three fiber coils (Fig.2).

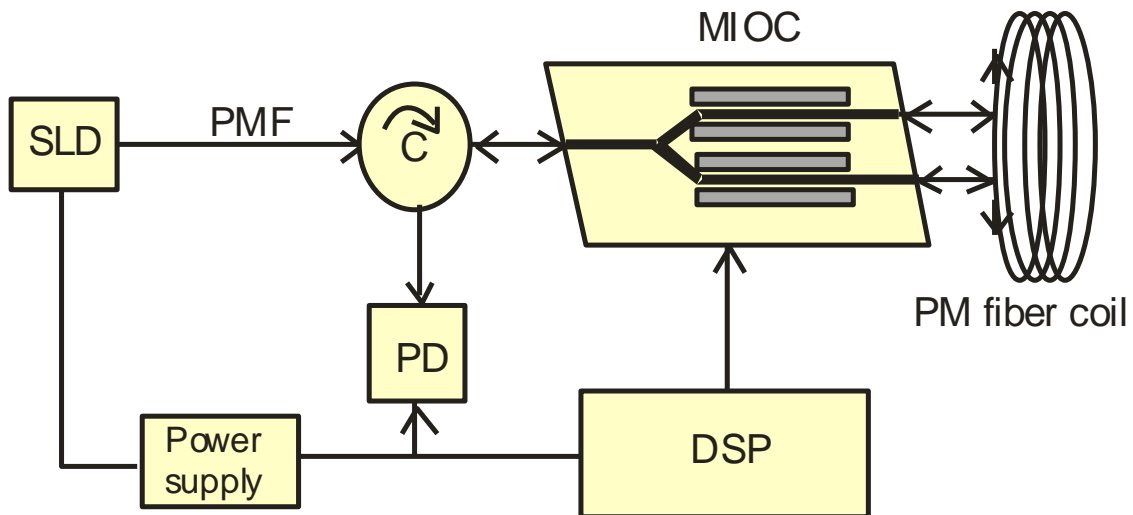


Fig.1. Single axis IFOG configuration.

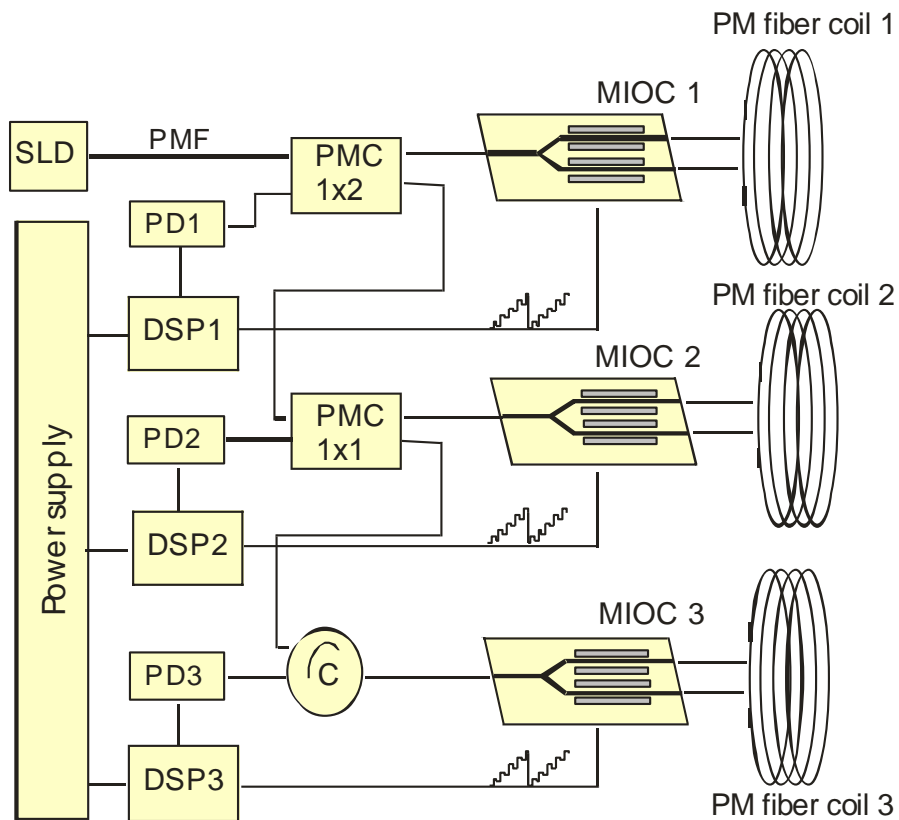


Fig.2. Three axis IFOG configuration.

2.2. Configuration of space grade IFOG

Beside fiber optical gyros for commercial application, the space grade three axis FOG named VOBIS, with performance 0.03 deg/h has been developed. Its configuration is shown at Fig.3. Only space grade electronic components were used in FOG. We tried to minimize the number of purchased optical components in our IFOG. The IFOG is comprising a some of optical devices: active optoelectronic component (SLED, PD and MIOC) and passive optical component (Polarizing Splitter (PS) and fiber coil for the Sagnac interferometer). As no space qualified alternative is available on the market, these optical devices were to be procured on commercial standard (Commercial Off The Shelf or COTS components) and upgraded to space standard. Fortunately, the main components (MIOC, PS, fiber coil and partially PD) are produced by Optolink. The SLED's used are taken from the Telecom Industry, and some qualification data (such as Telcordia qualification) were already available. The objective is then to procure a batch of components supposed equivalent and to qualify this batch with a representative sample. The qualification of the technology has been achieved in three steps: component procurement, qualification plan definition and qualification testing.

The main dependence of IFOG technology to space environment is radiation induced insertion loss in the fiber coil. This degradation of the optical power budget could lead the degradation of the IFOG Angular Random Walk. The special radiation hard fiber was developed and used in Optolink's FOG. We have developed the technology for forming fluorine-doped silica glass light-reflecting cladding with $\Delta n \sim -(8.5 - 9.5) \times 10^{-3}$ using SiF_4 as fluorine-agent.

Even if the qualification of FOG technology to space environment is not entirely finished, the key environmental tests have already been successfully achieved. With these precautions, good results have been obtained under radiation, ensuring above 15 years at geostationary orbit. The space launch of this FOG is expected to be done at the end of 2012.

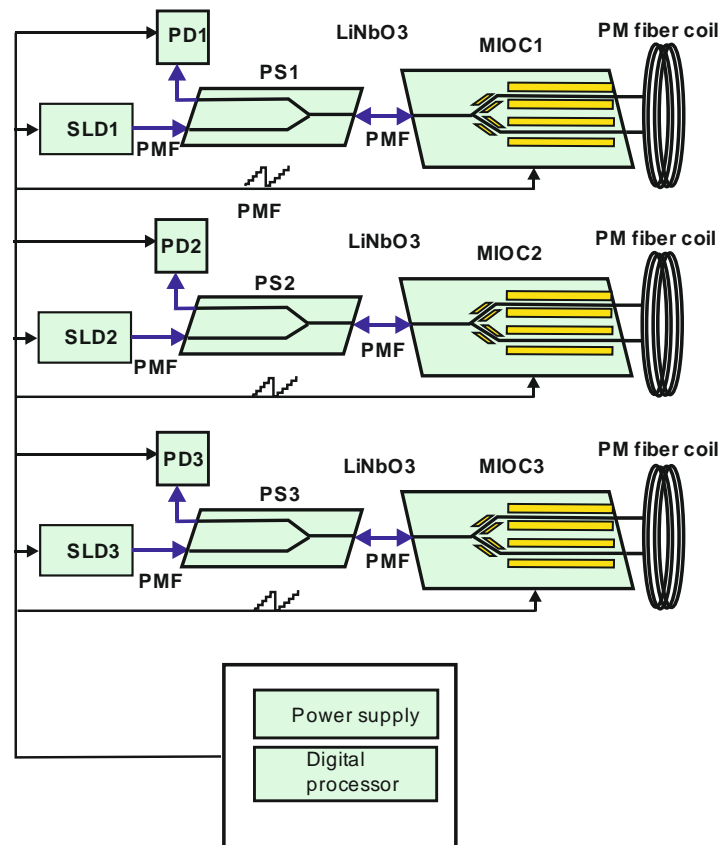


Fig.3. The 3-axis space grade IFOG (VOBIS) configuration.

2.3. PM fiber.

The accuracy of FOG depends strongly on parameters of optical block. The device noise is smaller the larger is output power of SLD and smaller optical losses at all optical components, including PM fiber. The minimal measured rotation rate depends on polarization crosstalk h and beat length L_p of PM fiber as following [3]:

$$\Omega_{\min} \sim \frac{\sqrt{hL_p}}{DL} \quad (2)$$

So, the main our activity was directed to reduce optical loss, polarization crosstalk and beat length in PANDA fibers.

Table 1 shows the present parameters of Optolink's PM fibers.

Table 1. Parameters of Optolinks PM fibers.

Operating wavelength	1.55 μm
Mode Field Diameter	From 6.5 to 9.5 μm
Cladding Diameter	From 80 to 125 μm
Coating Diameter	From 120 to 200 μm
Numerical Aperture	0.13-0.15
Polarization crosstalk (h-Parameter)	$<10^{-5} /\text{m}$
Attenuation	$< 2 \text{ dB/km}$
Cutoff Wavelength	1250nm-1450nm
Beat Length	$<3\text{mm}$
Stress Type	PANDA

The origin of radiation-induced attenuation in optical fibers is the color centers that are created by trapping of radiolytic electrons and holes by charged precursor defect centers, such as non-bridging oxygen, Si-Si bonds, and the presence of dopants or impurities. In the case of Ge-doped silica core fiber, Ge provides a large concentration of trapping sites, so the radiation-induced loss is dominated by Ge-related color centers. However, this large reservoir of trapping sites is absent in pure silica core (PSC) fibers, so second order effects become important. These include glass stoichiometry, the presence of low levels of impurities (including H and OH), stress due to fiber structure, glass consolidation, and draw conditions. The preform fabrication process also has an effect on radiation sensitivity. We have developed the technology for forming fluorine-doped silica glass light-reflecting cladding with $\Delta n \sim -(8.5 - 9.5) \times 10^{-3}$ using SiF_4 as fluorine-agent.

After formation of fluorine-doped silica glass cladding the SiO_2 fiber core is deposited inside supporting tube by SiCl_4 oxidation.

Optical fibers have been drawn out on drawing tower using high-temperature graphite heater with simultaneous covering with protecting and strengthening two-layer UV-curable acrylo-urethane coating coating. Silica fiber diameter $80 \pm 1,5 \mu\text{m}$.

The index profile for such fiber is shown at Fig.4.

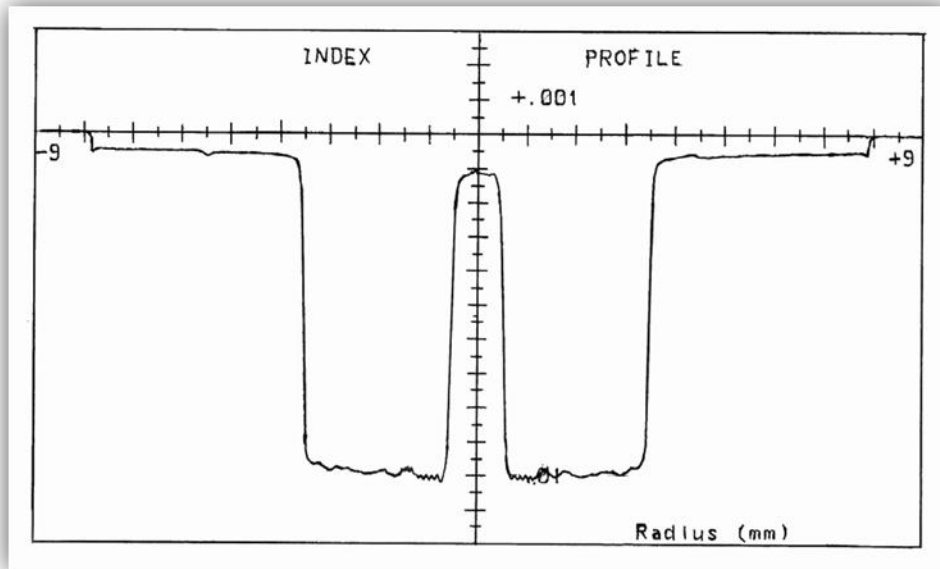


Fig.4. The refractive index profile of pure silica fiber.

Quadrupole winding technique implies winding a coil from a single length of fiber, starting at the center of the fiber length, winding outward toward the ends, alternately from one or another of two supply spools, in a geometrically structured way. Indeed, optical fiber is elastic but very delicate. Elasticity implies a need to keep fiber always under constant tension during winding. Delicacy implies a need to control not only in-process fiber tension, but also fiber flexure or curvature, and a surface contacts. The coil is placed at temperature isolated plate with diameter from 80 to 230 mm depending on type of FOG (see Table 2). Our fiber coil winding machine was specially developed basing on standard wire winding machine.

2.4. Integrated optical components

One of the main fiber optical gyroscope's components is a multifunctional integrated optical chip (MIOC). Optolink's MIOC is a solid state waveguide device on X-cut LiNbO_3 substrate fabricated by High-Temperature Proton Exchange method (HTPE) [2]. It includes a linear polarizer, Y-junction coupler and two pairs of electro-optic phase modulators. Light coming from the optical fiber coupler is linearly polarized within the MIOC to greater than 60 dB. This high degree of polarization minimizes bias uncertainty due to polarization non-

reciprocity. The Y-junction coupler within the MIOC splits the light into equal amplitude waves, each directed along a separate waveguide within the MIOC. Each of the resulting waves pass through a electrooptical phase modulator and after two waves counterpropagate around the optical PM optical fiber sensor coil.

A very important advantage of proton exchange (PE) waveguides is following. In such waveguides the extraordinary refraction index is increasing, while refraction index of ordinary ray is decreasing. As a result, proton exchanged waveguides support propagation only extraordinary polarization modes (TE in our case). Therefore, it is no necessity to use in the fiber optical gyroscope a polarizer, which brings additional loss.

It is well known, that standard technology of PE waveguide (APE-technology) [4] applies a two-level process, which consists of a PE, (melting pure or diluted by lithium benzoate benzoic acid as a rule) and subsequent annealing (Fig.4a). It was recently obtained, that different defects are formed in the surface area of waveguide due to different phase transitions [5]. These defects are sources of additional scattering of light.

In the paper [2] we reported the fabrication and characterization of LiNbO_3 optical waveguides prepared by HTPE process. HTPE process, in contrast to APE, is a one step process and does not allow any phase transitions (Fig.5), and, therefore, allows one to achieve the smaller optical losses and higher electro-optical coefficients.

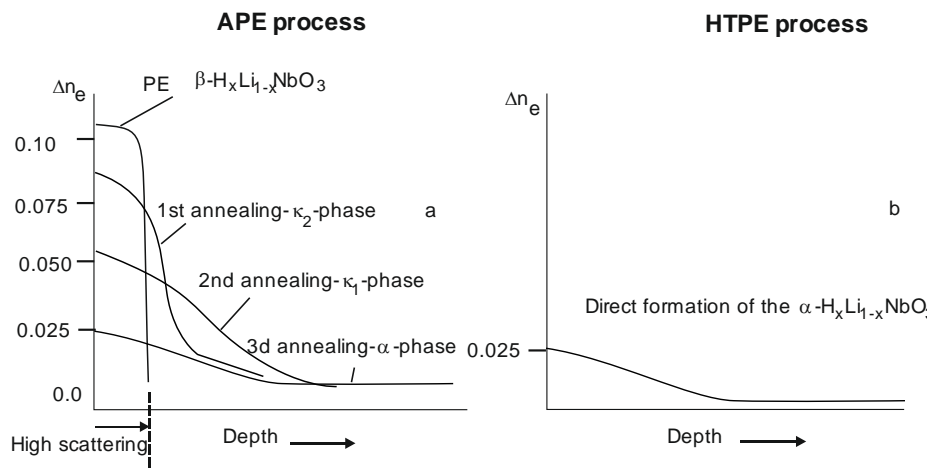


Fig.5. Formation of α -phase PE LiNbO_3 waveguides by APE (a) and HTPE (b) processes.

The HTPE processes are held in the specially developed containers. The specially developed metals and dielectric films used as masks to provide locality proton exchange diffusion. Then by vacuum deposition of electrodes, the integrated electro-optical phase modulators are formed on both arms of Y- splitter. Then the end surfaces are cut (the

angle is 10 degree to the Y axis), polished, and finally they are coupled with PM fiber pigtails. The final steps are packaging and welding electrodes.

The parameters of MIOC are following:

- half wave modulation voltage: < 3V
- polarization extinction ratio: < -50dB
- intensity modulation: < 0.1%
- insertion loss: < 4 dB

2.5. Block of electronics

Digital signal processor (DSP) generates voltage for “sawtooth” light modulation for compensation of Sagnac phase shift and to make fixed phase shift $\pi/2$. As a result, each channel is working in closed-loop regime. Fig.6 shows the scheme of DSP.

Analog signal from analog phase sensitive detector (PSD) that processes the output of the FOG photodetector is amplified and passed to high frequency analog to digital converter (ADC). The digital signal is demodulated by Altera Field Programmable Gate Array (FPGA). Obtained code passed to digital integrator. The code of signal from integrator is using to obtain the slop of phase “saw-tooth” which corresponds to rotation rate. The Digital to Analog converter creates the analog signal as saw-tooth voltage and pass it to MIOC. The wideband integrated optic phase modulators placed at both arms of MIOC are employed to introduce phase ramp modulation, thus enabling close-loop operation. The loop closure scheme uses a digitally synthesized saw-tooth (serrodyne modulation) of 2π amplitude in optical phase shift. In this case the Sagnac phase shift is compensated by saw-tooth modulation of light with calibrated amplitude 2π and frequency f , determined from well-known equation:

$$f = \frac{D}{n\lambda} \Omega$$

where Ω is a rotation rate, D – diameter of fiber coil, n - effective refractive index of waveguiding mode, λ - wavelength.

The frequency of resulting ramp is then a digital measure of the rotation rate, with each ramp reset proportional to the angular turned, i.e. one ramp is equal to $\frac{n\lambda}{D}$. To increase resolution of gyro the rotation rate is determined by measuring slop of phase saw-tooth.

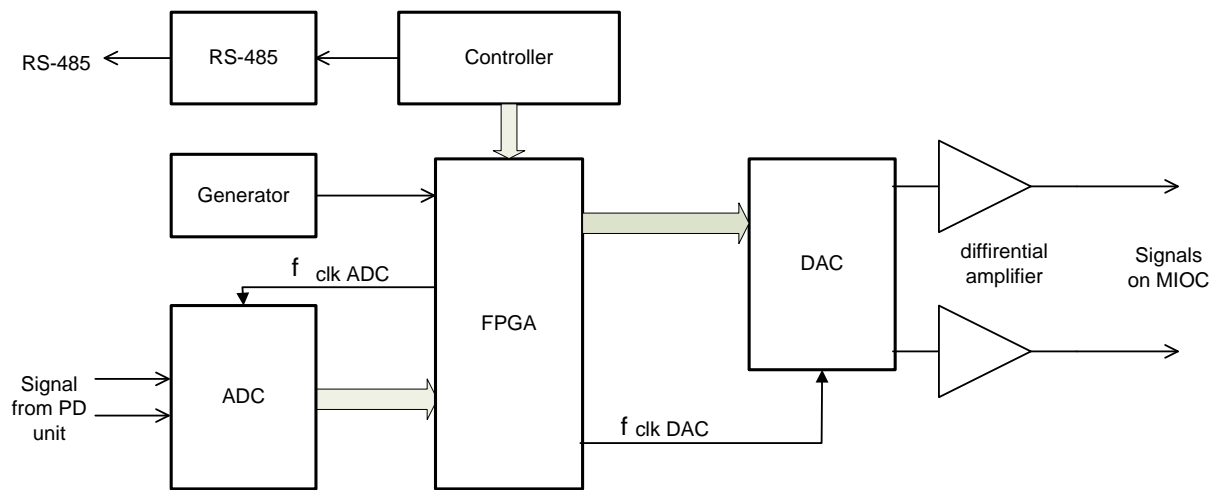


Fig.6. Block diagram of DSP.

ADC – analog digital converter, DAC – digital analog converter, FPGA – Field Programmable Gate Array, PD unit – photodetector unit.

DSP represents the circuit based on Altera's FPGA. DSP is connected with high-speed ADC and with two fast Analog Devices's DAC. Clock pulse for DAC and ADC are drawing up by FPGA. Work of FPGA are clocked by external thermo-stabilized generator.

On one of DSP the Atmel's microcontroller is established which is working as the loader for FPGA. Controller provides an exchange on interface RS-485 with external devices. The monitor for device settings is realized based on this controller. Except for loading FPGA, the controller reads out the data of measurements from FPGA.

The shaper of clock pulses transforms clock frequency to a set of impulses for synchronous work management of all devices and units. Clock frequency f_{clk} gets out to multiple frequency AM f_{am} . Clock pulses for DAC are formed on fronts AM. Clock pulses for ADC are formed so that to exclude measurements on fronts of a signal from PD.

The circuit of processing the signal coming from PD consists of the integration block, the buffer for storage of the measured value and the differencing circuit. The sum of the values of mismatch signal measured on the current phase AM is collected at integration block. On the buffer the sum of the values measured on previous phase AM is stored. After the measurements the values from the integration block and from the buffer pass to the differencing circuit. Depending on current phase of AM, one number passes as deducted and another as the subtractor. Thus the amplitude of a variable signal is allocated taking into account its sign.

The code with sign, corresponding to a sign of a mismatch signal, passes to the digital integrator which consists of the multiplier and the summing unit with the circuit of

restriction. The time constant of the digital integrator is setting by the multiplier. The summing unit is used as the integrator. The code from the integrator passes to the shaper of the code for compensating modulation and through the digital filter to the serial interface of connection with the controller.

The shaper of a code for compensating modulation includes the summing unit which forms the "saw-tooth" code and the second summing unit which is used in a contour of a digital regulator of amplitude of compensating modulation. The signal from the circuit of processing of a signal from PD taken off at the moment of recessions of "saw-tooth" serves as signal of a mismatch for a digital regulator of amplitude of compensating modulation. The same signal is used for fine tuning of amplitude of auxiliary modulation.

There are two main sources of scale factor errors: (i) the finite flyback time and (ii) the nonstability of phase amplitude. To avoid influence of first factor we used the special transformation in the circuit, which creates a control voltage signal for MIOC. In our scheme the flyback time excludes from transmission characteristics of electro-optical modulator. The nonstability of phase amplitude is minimized by creating the astatic follow-up system. The response of device on periodic signal with calibrated constant period is considered as an error signal. Special circuit, independently on FOG moving, generates this periodic signal securing the zero error of stabilization of phase saw-tooth at 2π value at stationary rate and negligibly small error of this value at dynamic rate.

2.6. IFOG performance.

In our design we reduce as much as possible the fundamental limitation of IFOG performance:

Optical losses

Sensitivity of IFOG is limited by shot noise that goes as the square root of the power that decreases with fiber length. However, the Sagnac effect increases with the length of the fiber. These two competing effects set the length of the fiber for a given sensitivity.

Thermal Noise

Time dependent temperature gradient along the length of the fiber can introduce spurious phase shifts due to the temperature dependence of the refractive index of fiber. To minimize this effect the fibers with smaller dn/dT dependence should be used. Also, quadropole winding such that equidistant points from fiber center are physically close to each other strongly reduce this effect.

Backscattering of light

Backscatter at the output-input couplers and MIOC faces can interfere with the main beams creating parasitic interferometers. Immersion cell to reduce index of refraction step as well as using of tilted MIOC faces reduce backscattering.

Optical Kerr Effect

Electric fields of the counter-propagating beams can cause changes in the index of refraction that is nonreciprocal if light is splitting at unequal parts. The nonreciprocity induced by the nonlinear Kerr effect can be strongly reduced with improving of MIOC technology.

Magneto-optical effect

The magneto-optical Faraday effect is a nonreciprocal effect which is potentially dangerous in adding to the Sagnac effect. This problem is now almost solved by the use of carefully untwisted polarization maintaining fibers as well as by using cases from special materials.

For the IFOG with perfect components (ideal splitter, no backscattering, etc.), the measurement limit is imposed by the shot noise in the light as measured by photodetector. The uncertainty $\delta\Omega_\pi$, generated by the fluctuation in the light due to shot noise can be expressed as [6]:

$$\delta\Omega_\pi = \frac{c}{L \cdot D} \frac{\lambda/2}{(n_p n_D \tau)^{\frac{1}{2}}}$$

where n_p is the number of photons per second coming to photodetector, n_D is detector quantum efficiency and τ is averaging time.

The main parameters of produced and commercially available Optolink's FOGs [7-13] are presented at Fig.7 and Table 2.

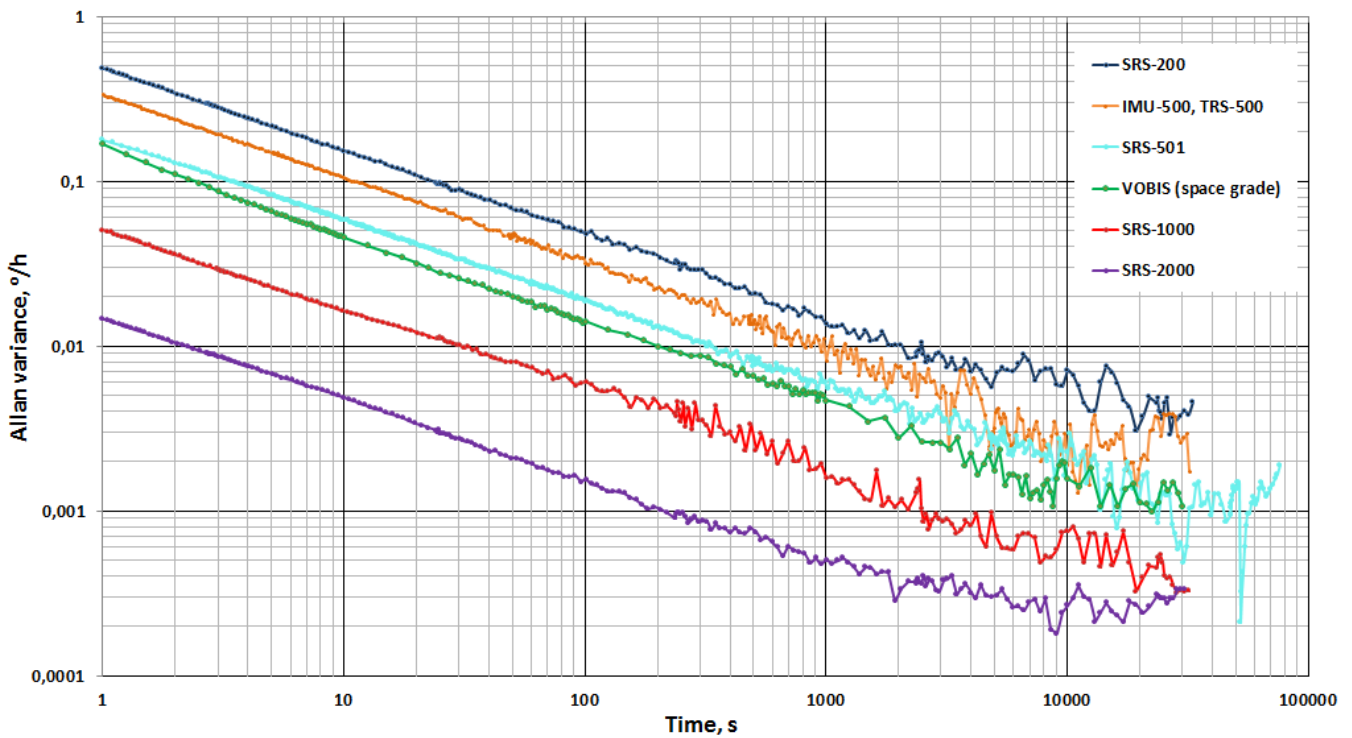


Fig.7. Allan variance for Optolink's IFOGs.

Table 2. Parameters of Optolink's fiber optical gyroscopes.

Parameter	Single axis SRS-2000	Single axis SRS-1000	Single axis SRS-501	Three axes TRS-500	Single axis SRS-200	Three axis VOBIS Space grade
Range of measured angular rate, deg/sec	±40	±90	±250	±300	±800	±30
Bias drift at fixed temperature, deg/h	0.005	0.01	0.1	0.1	0.2	0.03
Scale factor repeatability, ppm	100	200	500	700	1000	500
Bandwidth, Hz:	50	100	300	300	400	100
Random walk, deg/√h	0.0003	0.0005	0.003	0.01	0.02	0.001
Weight, kg	1.1	0.8	0.35	1.2	0.22	2.6
Dimensions, mm:	Ø 250x80	Ø150x80	Ø100x30	110x110x90	Ø70x28	172x176x110

References

- [1] H.Lefevre, "The Fiber Optic Gyroscope", Artech House, (1993).
- [2] Yu.N. Korkishko, V.A. Fedorov, O.Y.Feoktistova. "LiNbO₃ optical waveguide fabrication by high-temperature proton-exchange", IEEE J. Lightwave Technol., 2000, Vol.18, pp.562-568.
- [3] "Optical Gyros and their Application", RTO – AG, 339, 1999.

- [4] P.G. Suchoski, T.K. Findakly, F.J. Leonberger. "Stable low-loss proton-exchanged LiNbO₃ devices with no electro-optic degradation" // Opt. Lett., 1988, Vol.13, pp.1050-1052.
- [5] Yu.N. Korkishko, V.A. Fedorov. "Structural Phase Diagram of H_xLi_{1-x}NbO₃ waveguides: The Correlation Between Structural and Optical Properties" // IEEE Journal of Selected Topics in Quantum Electronics, 1996, Vol.2, No 2, pp.187-196.
- [6] J.L. Davis, S. Ezekiel, "Techniques for shot-noise limited inertial rotation measurement using a multiturn fiber Sagnac interferometer" // Proc. SPIE, 1978, Vol.157, pp.131–137.
- [7] V.E. Prilutzkii, Yu.K. Pylaev, A.G. Gubanov, Yu.N. Korkishko, V.A. Fedorov, E.M.Paderin, High-Precision Fiber Optical Gyroscope with Linear Digital Output // in Proc. 9th Saint Petersburg International Conference on Integrated Navigation Systems, Saint Petersburg, May 27-29, 2002, pp.333-342.
- [8] Yu.N.Korkishko, V.A.Fedorov, S.M.Kostritskii, A.N.Alkaev, E.M. Paderin, E.I.Maslennikov, D.V.Apraksin. Multifunctional integrated optical chip for fiber optical gyroscope fabricated by high temperature proton exchange // in Proc.SPIE, Vol.4944, Integrated Optical Devices: Fabrication and Testing, edited by Giancarlo C. Righini, (SPIE, Bellingham, WA, 2003), pp. 262-267.
- [9] V.E. Prilutsky, V.G.Ponomarev, V.G.Marchuk, M.A.Fenyuk, Yu.N. Korkishko, V.A. Fedorov, S.M.Kostritskii, E.M.Paderin. Interferometric Closed-Loop Fiber Optic Gyroscopes with Linear Output // in Proc. 11th Saint Petersburg International Conference on Integrated Navigation Systems, Saint Petersburg, May 24-26, 2004, pp.252-258.
- [10] Yu.N. Korkishko, V.A. Fedorov, V.E. Prilutsky, V.G.Ponomarev, V.G.Marchuk, I.V.Morev, E.M.Paderin, S.M.Kostritskii, V.N.Branets, V.S.Ryzhkov. Three-axis Fiber Optical Gyroscope for Rocket&Space Applications // in Proc. 13th Saint Petersburg International Conference on Integrated Navigation Systems, Saint Petersburg, May 29-31, 2006, pp.237-242.
- [11] Yu.N. Korkishko, V.A. Fedorov, V.E. Prilutskii, V.G. Ponomarev, V.G.Marchuk, I.V.Morev, S.M.Kostritskii, E.M. Paderin, L.P.Nesenyuk, A.S.Buravlev, L.G.Lisin. Navigation-Grade Interferometric Fiber Optical Gyroscope // in Proc. 14th Saint Petersburg International Conference on Integrated Navigation Systems, Saint Petersburg, May 28-30, 2007, pp.138-143.
- [12] A.V.Chernodarov, A.P.Patrikeev, Yu.N.Korkishko, V.A.Fedorov, S.E. Perelyaev. Software Seminal Development for FOG Inertial Satellite Navigation System SINS-500 // Gyroscopy and Navigation, 2010, Vol. 1, No. 4, pp. 330–340.

[13] Yu.N. Korkishko, V.A.Fedorov, V.E.Prilutskii, V.G.Ponomarev, I.V.Morev, S.M.Kostritskii. Interferometric closed-loop fiber-optic gyroscopes // in Proc.SPIE, Vol.8351, Third Asia Pacific Optical Sensors Conference, edited by John Canning, Gangding Peng, (SPIE, Bellingham, WA, 2012), 83513L, pp. 83513L-1–83513L-8 (2012).